

Detection and Attribution of Twentieth-Century Northern and Southern African Rainfall Change

MARTIN HOERLING

NOAA/Earth System Research Laboratory, Boulder, Colorado

JAMES HURRELL

National Center for Atmospheric Research, Boulder, Colorado*

JON EISCHEID

NOAA/Earth System Research Laboratory, Boulder, Colorado

ADAM PHILLIPS

National Center for Atmospheric Research, Boulder, Colorado*

(Manuscript received 20 January 2005, in final form 30 November 2005)

ABSTRACT

The spatial patterns, time history, and seasonality of African rainfall trends since 1950 are found to be deducible from the atmosphere's response to the known variations of global sea surface temperatures (SSTs). The robustness of the oceanic impact is confirmed through the diagnosis of 80 separate 50-yr climate simulations across a suite of atmospheric general circulation models. Drying over the Sahel during boreal summer is shown to be a response to warming of the South Atlantic relative to North Atlantic SST, with the ensuing anomalous interhemispheric SST contrast favoring a more southern position of the Atlantic intertropical convergence zone. Southern African drying during austral summer is shown to be a response to Indian Ocean warming, with enhanced atmospheric convection over those warm waters driving subsidence drying over Africa.

The ensemble of greenhouse-gas-forced experiments, conducted as part of the Fourth Assessment Report of the Intergovernmental Panel on Climate Change, fails to simulate the pattern or amplitude of the twentieth-century African drying, indicating that the drought conditions were likely of natural origin. For the period 2000–49, the ensemble mean of the forced experiments yields a wet signal over the Sahel and a dry signal over southern Africa. These rainfall changes are physically consistent with a projected warming of the North Atlantic Ocean compared with the South Atlantic Ocean, and a further warming of the Indian Ocean. However, considerable spread exists among the individual members of the multimodel ensemble.

1. Introduction

Perhaps no large-scale monsoon system is more responsive to the worldwide distribution of ocean temperatures than that of Africa. Drought during July–

August–September (JAS) over the Sahel was originally shown to be associated with warm sea surface temperatures (SSTs) in the South Atlantic Ocean and the Gulf of Guinea (Lamb 1978a,b; Hastenrath 1984). Subsequent discoveries revealed a near-global scale to the SST anomalies. Folland et al. (1986) demonstrated that persistently dry and wet periods over the Sahel were accompanied by an interhemispheric contrast in SSTs: drought (pluvial) periods are linked to warm (cold) SST states of the Southern Hemisphere relative to those of the Northern Hemisphere. The interpretation of their results as denoting a causal, and potentially predictable, relation was supported by subsequent modeling efforts (Palmer 1986; Rowell et al. 1995).

* The National Center for Atmospheric Research is sponsored by the National Science Foundation.

Corresponding author address: Martin Hoerling, NOAA/Earth System Research Laboratory, R/PSD1, 325 Broadway, Boulder, CO 80305-3328.
E-mail: martin.hoerling@noaa.gov

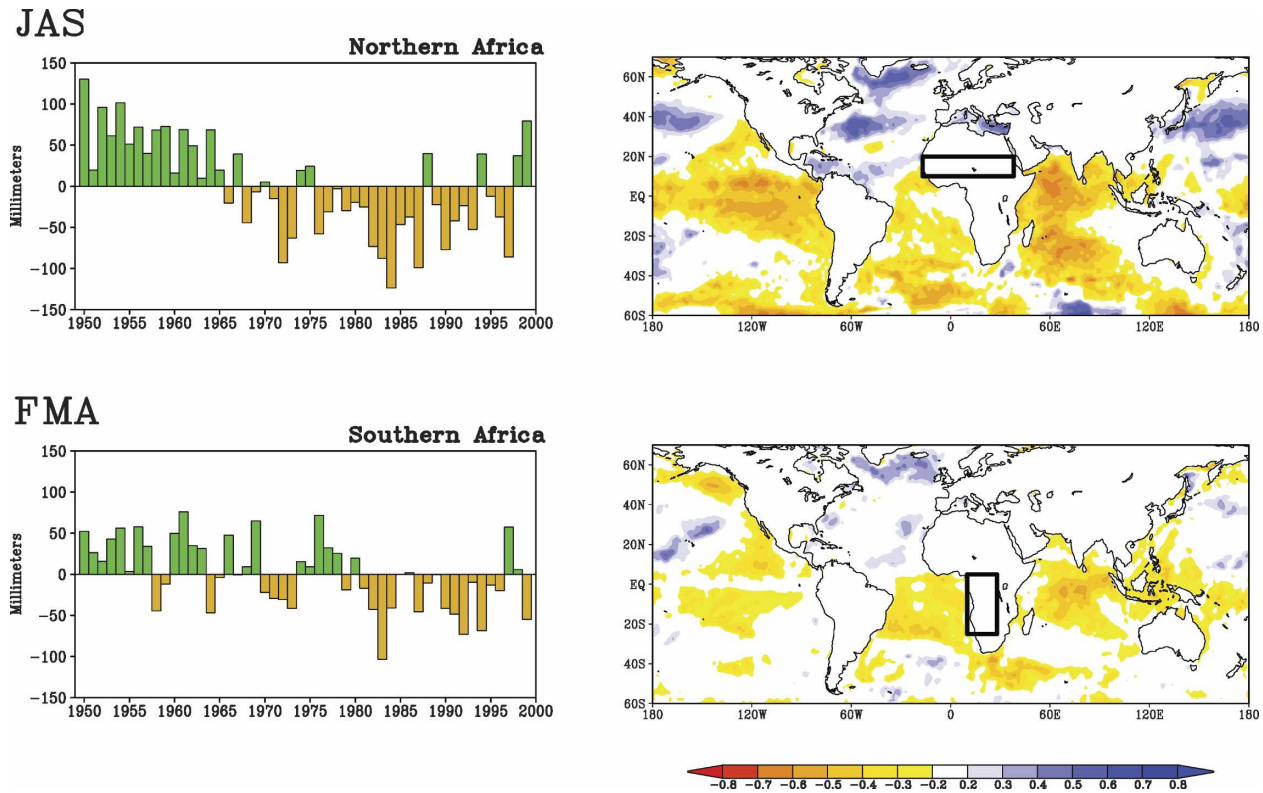


FIG. 1. Seasonal time series of observed 1950–99 rainfall departures for (top left) JAS over northern Africa and (bottom left) FMA over southern Africa. Rainfall is based on the monthly, gridded Climate Research Unit data. (right) The spatial averaging regions are indicated by black boxes. The 1950–99 temporal correlation between each rainfall time series and global SSTs for (top right) the JAS northern African rainy season and (bottom right) the FMA southern African rainy season.

The austral summer rains of southern Africa are also known to be sensitive to the state of global SSTs, including variations over the equatorial east Pacific Ocean (e.g., Mason et al. 1999; Landman and Goddard 2002), the Indian Ocean (Goddard and Graham 1999), and the South Atlantic Ocean (e.g., Hirst and Hastenrath 1983; Rouault et al. 2002). A trend toward increased aridity since 1950 has emerged over southern Africa (Hulme 1996). A 20% reduction in the climatological February–March–April (FMA) rainfall has been observed since 1950 there, compared with a 35% reduction over the same period for the Sahel.

The 1950–99 time histories of northern and southern Africa rainfall during their respective wet seasons are well described by linear downward trends (Fig. 1). A correlation of each time series with SSTs gives the impression that drying over both regions has similar oceanic ties (Fig. 1). A striking common feature is the warm SSTs throughout the Tropics associated with drying during both seasons, a pattern resembling the 1950–99 SST trend pattern itself.

This paper explores the nature and causes for the regional downward trajectories of African rainfall.

Have significant changes been detected that are unlikely to have occurred by chance? For instance, are these drying trends consistent with natural variability alone, in particular the intrinsic variations of the coupled ocean–atmosphere system? Which air–sea interactions have been most relevant, and are the secular drying trends during each monsoon season attributable to common oceanic influences, as implied in Fig. 1?

Clarity on these problems is a prerequisite to understanding possible human influences on African climate. Regarding the role of oceans, it is possible that anomalous air–sea interactions to which African rainfall is sensitive could be initiated by changes in the atmosphere’s chemical composition. Among the major conclusions of the Third Assessment Report of the Intergovernmental Panel on Climate Change (IPCC; Houghton et al. 2001) is that the observed globally averaged surface warming since 1950 is likely because of increased greenhouse gas concentrations (e.g., Barnett et al. 2005). Regional warming of the tropical sea surface also appears attributable to anthropogenic origins. Knutson et al. (1999) find recent warming rates of the Indian and South Atlantic Oceans exceed those ex-

pected from natural variability, and Stott et al. (2000) independently support this conclusion. A question we explore is whether the downward trajectory of African summer rainfall since 1950 is a consequence of the upward trajectory in tropical SSTs. Can the twentieth-century African rainfall trends be attributed to dynamical feedbacks, involving air–sea interactions, which were triggered by anthropogenic forcing?

The basis for our detection and attribution is large, ensemble suites of climate simulations employing several different general circulation models. Using one of these, Giannini et al. (2003) provided compelling evidence that the recent JAS drying trend over the Sahel is consistent with a sensitivity to global SSTs (see also Paeth and Hense 2004). Giannini et al. (2003) also found the drying to be statistically linked with Indian Ocean SSTs, from which they proposed that a late twentieth-century Indian Ocean warming trend might have caused the Sahelian drying trend. This interpretation gathers some support from experiments by Bader and Latif (2003) and Lu and Delworth (2005), although the earlier simulations of Palmer (1986) yielded drying only over the far eastern Sahel in response to Indian Ocean warmth. The question thus remains open whether the strong correlation between Sahel drought and Indian Ocean warmth (Fig. 1) is merely coincidental. Also unclear is whether warm states of the Indian Ocean exert similar influences on both boreal and austral summer African rains.

We employ a multimodel approach to gain insight on these questions and to quantify the robustness of oceanic impacts on African rainfall. In particular, we examine the African rainfall sensitivity to the observed variations in global SSTs during the last half of the twentieth century using five different atmospheric general circulation models (AGCMs). The models, their experimental design, and an appraisal of their capacity to simulate the climatological African rainfall are discussed in section 2. Results are presented in section 3, including a diagnosis of the probabilistic aspect of the AGCM simulated rainfall trends and a comparison with 50-yr rainfall trends occurring in long integrations of unforced coupled ocean–atmosphere models. Section 4 explores the role of specific SST forcings using idealizations of the global SST history since 1950, and we focus on the role of Atlantic and Indian Ocean changes. Section 5 examines the extent to which African rainfall trends during 1950–99 are attributable to greenhouse gas forcing, and whether these recent dryings are harbingers of twenty-first-century change. A discussion of outstanding questions regarding recent and future African rainfall changes appears in section 6, with concluding remarks given in section 7.

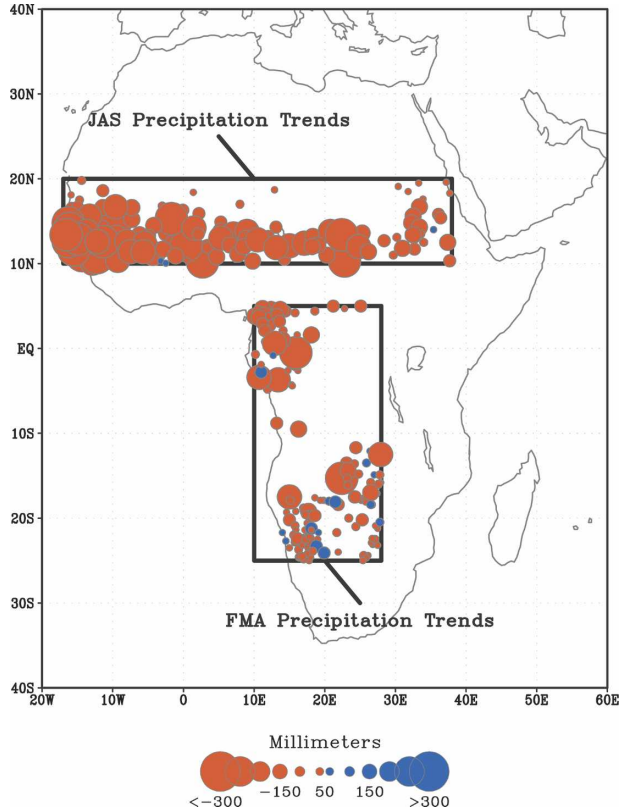


FIG. 2. Observed seasonal rainfall trends during 1950–99 for all available stations within the northern and southern African index regions. Station locations indicated by circles, with dry (wet) trends denoted by red (blue), and the intensity of trends indicated by a circle's size. Station values of monthly rainfall are based on the Global Historical Climate Network, and the circles denote all sites having at least 40 yr of measurements during 1950–99.

2. Data

a. Observations

Observed monthly rainfall data are available on a 0.5° grid, and the input observations together with the gridding methodology are described in Legates and Willmott (1990) and Willmott and Robeson (1995). Uncertainty in rainfall trend estimates comes from the fact that station measurements are typically unavailable at such high resolution, and the measurements are often not continuous over the full 1950–99 period. That a *qualitative* decline occurred in summer African rainfall since 1950 is supported by analysis of historical climate network stations having at least 40 yr of records (Fig. 2).

Monthly SST analyses come from the Met Office Hadley Centre's Global Sea Ice and SST dataset (Rayner et al. 2003). The global SSTs were created using various techniques including reduced space optimal interpolation, and they are available on a 1° grid.

TABLE 1. The characteristics of five different atmospheric GCMs used in this study. Further details of each model can be found in the listed references.

	Horizontal resolution	Vertical resolution	Ensemble size	References
CAM2	T42	18	15	Kiehl and Gent (2004)
ECHAM4.5	T42	18	24	Roeckner et al. (1996)
ECHAM3	T42	18	10	Roeckner et al. (1992)
NSIPP-1	$2.2 \times 5, 3^\circ \times 3.75^\circ$	34	23	Schubert et al. (2004)
ARPEGE	T63	31	8	Cassou and Terray (2001)

b. Atmospheric climate simulations forced by global SSTs

Sea surface forcing of climate variability is assessed using AGCMs forced with the specified, observed monthly variations in SSTs and sea ice concentrations for 1950–99. Ensemble methods are employed in which multiple integrations are begun from different atmospheric initial conditions, but subjected to identically specified sea surface conditions. The ensemble mean and the spread among members are analyzed so as to measure the uncertainty in our attribution of the oceanic role. We illustrate such statistical behavior within an ensemble by constructing its probability density function (PDF). Table 1 summarizes the spatial resolutions of the AGCMs we employ. The reader is referred to the indicated references for details on the different dynamical cores and physical parameterizations used in each model. A total of 80 simulations spanning the last half of the twentieth century are used in our analysis.

Comparisons of the annual mean and the first harmonic of African rainfall with observations are shown in Fig. 3. The major features of the multimodel climatology are common to the five individual AGCMs (not shown). The pattern of annual mean rainfall includes a maximum over equatorial Africa and the Gulf of Guinea, and a strong rainfall gradient separating the more humid areas south of 15°N from the desert reaches north of 20°N . This transition zone is commonly referred to as the Sahel region, and it is realistically delineated in the simulations.

Most of the annual mean rainfall over the Sahel (10° – 20°N) falls during JAS. The simulations realistically capture the seasonal timing and amplitude of this northern African monsoon, as they do for the December–March seasonal rainfall maximum over southern Africa (Fig. 3, right panels). In general, the simulated annual rainfall totals exceed those observed, especially over equatorial and southeastern Africa.

Another desirable attribute is the ability of AGCMs to skillfully simulate the interannual variations of seasonal African rainfall. Rowell et al. (1995) had previously demonstrated the high skill of simulations for

10 individual years of extreme Sahel rainfall. The 50-yr-averaged simulation skill for each of the models used herein, for both the Sahel in JAS and southern Africa in FMA, is found to be statistically significant at 95% (Table 2). Furthermore, each model produces drying trends in the two regions that are in quantitative agreement with observations. Our subsequent analysis is largely drawn from the multimodel averaged data, with the recognition that similar results emerge from the each of the individual AGCMs.

c. Atmospheric climate simulations forced by idealized SSTs

Simulations using a fixed Indian Ocean positive SST anomaly, the pattern and strength of which is an idealization of the 1950–99 SST trend, are conducted. The idealized SST anomaly has a maximum amplitude of $+1^\circ\text{C}$ between 5°S – 5°N , which is reduced to zero amplitude at 25° latitude. This anomaly pattern is specified and fixed throughout the seasonal cycle and is added to the seasonally varying climatological SSTs. Twenty 14-month simulations, beginning from randomly selected 1 November atmospheric initial conditions, were performed with the National Center for Atmospheric Research (NCAR) Community Atmospheric Model, version 2 (CAM2), and twenty 18-month simulations were performed using the identical anomalous SST forcing with the National Aeronautics and Space Administration (NASA) Seasonal-to-Interannual Prediction Project (NSIPP-1) model. (The NSIPP-1 experiments and data were kindly provided by Drs. P. Pegion, M. Suarez, and S. Schubert.)

A third ensemble of experiments is forced only by the monthly evolving SST history of the entire Atlantic Ocean since 1950. The runs are based on the joint Météo-France and European Centre for Medium-Range Weather Forecasts Action de Recherche Petite Echelle Grande Echelle (ARPEGE) model from which a four-member ensemble was made available. (The ARPEGE experiments and data were kindly provided by Dr. C. Cassou.)

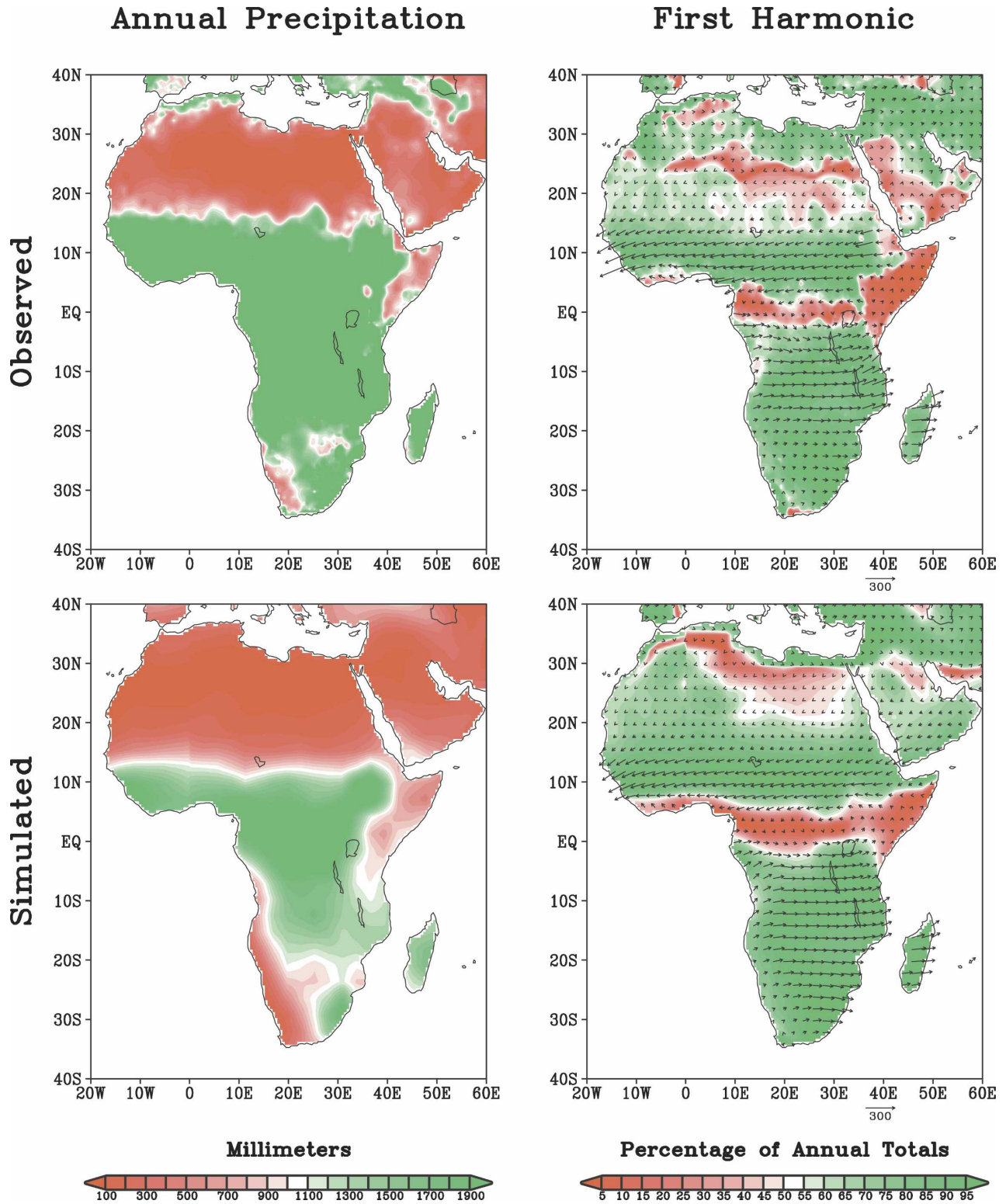


FIG. 3. African climatological (left) annual mean rainfall (mm) and (right) the first harmonic of climatological monthly rainfall (% of annual total rainfall). Arrows indicate the monthly peak in the first harmonic, with eastward (westward) pointing vectors denoting January (July) maxima.

TABLE 2. The 1950–99 trends, expressed as the total change relative to each model's 1950–99 climatology, of JAS and FMA rainfall for the five GCMs used in this study. The 50-yr trend of the multimodel and observations is also indicated. The interannual relationship between the rainfall of each model and observations is indicated by the 50-yr correlation coefficient. For JAS, the rainfall index is the area average over the Sahel (10°–20°N, 17°W–38°E) whereas FMA is the area average over southern Africa (5°N–25°S; 15°–40°E).

	JAS		FMA	
	Trend	Interannual	Trend	Interannual
ARPEGE	–32%	0.60	–15%	0.32
CAM2	–16%	0.30	–5%	0.32
ECHAM3	–24%	0.60	–7%	0.45
ECHAM4	–25%	0.51	–8%	0.57
NASA	–14%	0.77	–13%	0.38
Multimodel	–23%	0.59	–10%	0.52
Observations	–35%	—	–22%	—

d. Unforced coupled ocean–atmosphere climate simulations

Unforced, control integrations of three different coupled ocean–atmosphere models are diagnosed. These are the EC Hamburg/Ocean Pycnal (ECHAM4/OPYC; Roeckner et al. 1999) whose atmospheric component is similar to the one studied here using specified SSTs, the NCAR Coupled Climate System Model, version 2 (Kiehl and Gent 2004), whose atmospheric component is CAM2, and the Hadley Centre Coupled Model, version 3 (Gregory and Lowe 2000). For each coupled model, 240-yr simulations are used.

e. Forced coupled ocean–atmosphere climate simulations

Coupled ocean–atmosphere models forced with estimated greenhouse gas (GHG) and aerosol changes through 1999 and with the IPCC Special Report on Emissions Scenarios (SRES) A1B scenario (Houghton et al. 2001) thereafter are diagnosed from 18 different climate modeling groups around the world. These runs were done in support of the IPCC Fourth Assessment Report (AR4). The GHG signal is estimated by averaging the 18-model ensemble means. A total of 47 simulations spanning 1950–99, and 42 projections for 2000–49 are further diagnosed to determine the empirical distributions of simulated trends. The data were collected from the Program for Climate Model Diagnosis and Intercomparison (PCMDI) archive as part of the Coupled Model Intercomparison Project (more information available online at <http://www-pcmdi.llnl.gov/old/cmip>).

3. African rainfall response to 1950–99 observed global SST variations

Both the low-frequency time evolution of African rainfall since 1950 and the spatial structure of the 50-yr trends are attributable to global SST forcing (cf. Figs. 4 and 1). This is true for both the northern and the southern African regions, where the simulated trends are statistically significant at 99%. The simulated rainfall decline is –23% of the seasonal mean over the Sahel and –10% over southern Africa. Also shown in the right panels of Fig. 4 are the temporal correlations between the simulated seasonal rainfall with observed SSTs during 1950–99. Warm SSTs throughout the Tropics coincide with simulated dry conditions over Africa, and a particularly strong association with warm Indian Ocean SSTs is reminiscent of the findings of Giannini et al. (2003).

The spatial structure of the boreal summer monsoon drying, with a strong focus over the Sahel, is also consistent with a response pattern to global SST forcing (Fig. 5). Furthermore, each of the simulations produces a drying trend averaged over the Sahel. This is illustrated by the PDF of 50-yr trends averaged over 10°–20°N calculated from the 80 individual experiments (right panel, red curve). The observed drying trend thus appears to have been uniquely determined by the global SSTs, although the amplitude of the drying varies among the individual runs, with some exceeding the observed drying rate.

A drying trend follows the seasonal movement of the rains into southern Africa (Fig. 6; see also Figs. A1 and A2 for a complete display of the seasonal cycle of observed and simulated seasonal rainfall trends). As for JAS, a close correspondence between the observed (left panel) and the simulated (middle panel) trends affirms the ocean's role in the increased aridity. Drying has not occurred over tropical eastern Africa and, interestingly, the positive rainfall trend observed there is also consistent with an SST forced change. Once again, the sign of rainfall trends appear to have been virtually determined by the history of global SSTs: 79 of the 80 realizations yield a drying trend over southern Africa (right panel, red curve).

Have these observed 50-yr drying trends been the consequence of natural climate variability? They are consistent with, and in large part a consequence of, the particular trajectory in twentieth-century SSTs. This interpretation is based on the fact that the observed drying trends fall within the distribution function of simulations for 1950–99 (cf. red PDFs with the lengthened tick marks in Figs. 5 and 6). The question thus turns to

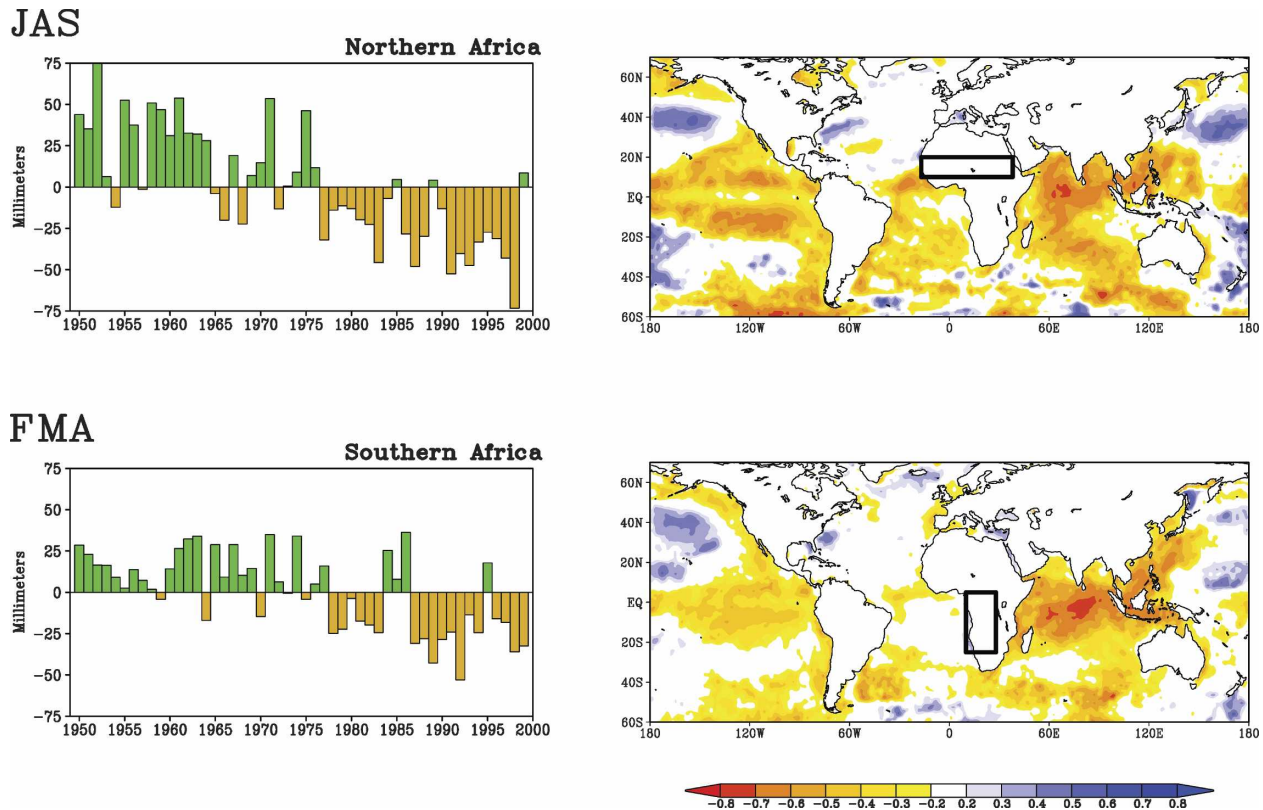


FIG. 4. Same as in Fig. 1 but for the seasonal time series of simulated 1950–99 rainfall departures for (top left) JAS over northern Africa and (bottom left) FMA over southern Africa. Rainfall is based on the monthly, gridded output of a multimodel, 80-member ensemble average of atmospheric GCM runs forced by the time-varying, monthly observed global SSTs. The 1950–99 temporal correlation between the ensemble mean simulated rainfall time series and global SSTs for (top right) the JAS northern African rainy season and (bottom right) the FMA southern African rainy season.

which SST variations are of importance, and whether those can be reconciled with natural variability.

The possibility that the observed rainfall trends are not the sole consequence of natural variations is supported by the fact that no single 50-yr trend in unforced coupled ocean–atmosphere models yields such drying rates (cf. blue PDFs with lengthened tick marks in Figs. 5 and 6). Likewise, nearly half of the AGCM simulated 1950–99 monsoon rainfall trends fall outside the coupled model’s PDF. This possibility must be tempered, however, by the realization that the current generation of coupled models does not offer a completely accurate picture of natural low-frequency variability. Their mean SST biases are well known, as is their failure to realistically simulate the El Niño–Southern Oscillation (ENSO) phenomenon (e.g., Achutarao and Sperber 2002). We have also found the particular models studied herein to possess weaker extratropical decadal SST variations than seen in observations (not shown). Another suggestion that they may have insufficient oceanic low-frequency variations emerges from

comparing the AGCM (red curves) and coupled model (blue curves) PDFs (Figs. 5 and 6). Aside from the difference in mean values, their distributions otherwise have similar spreads. In the case of the AGCMs, the spread is mostly due to *intrinsic atmospheric noise*: each run experienced identical specified SST variability. Of course, SSTs are not constrained in the coupled runs, so those simulations are free to generate different low-frequency SST evolutions. The fact that a comparable spread exists in the coupled models implies that such *intrinsic oceanic noise* is either small and/or is not contributing to multidecadal African rainfall change. We suspect this to be more a reflection of model deficiencies rather than a true measure of the ocean’s role (e.g., Barnett 1999).

4. African monsoon response to idealizations of 1950–99 global SST variations

The question of the Indian Ocean’s role in African climate change is particularly intriguing because its

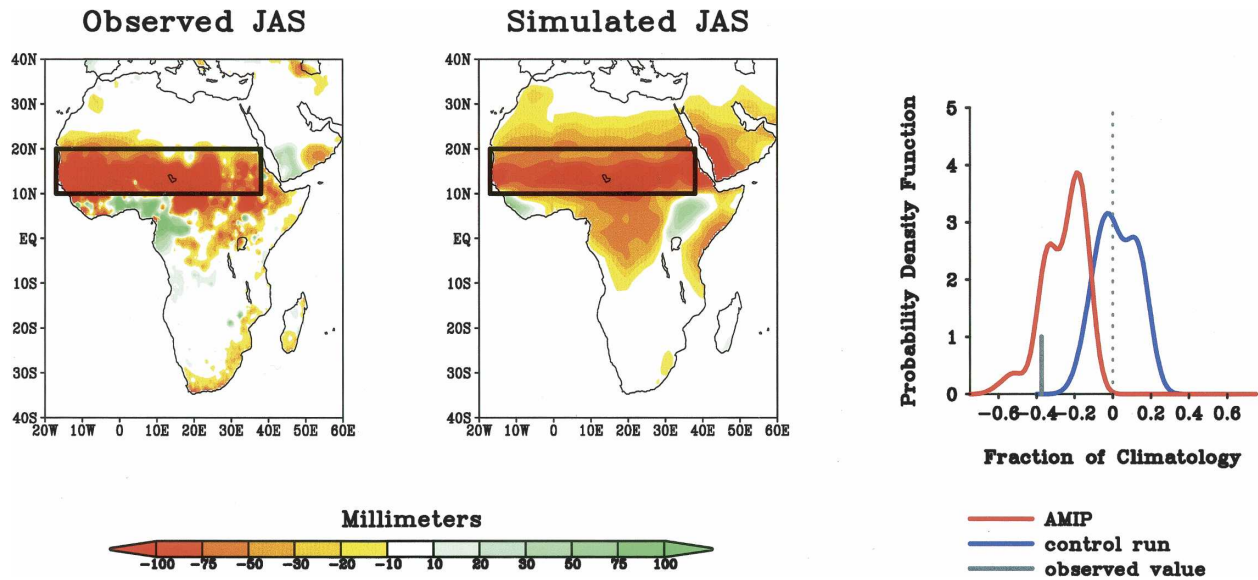


FIG. 5. The 1950–99 trends of (left) observed and (middle) atmospheric GCM simulated seasonal African rainfall for JAS. Plotted is the total seasonal rainfall change (mm) over the 50-yr period. (right) The empirical PDFs of JAS 50-yr rainfall trends averaged over the Sahel region. The data given by the red curve are from the 80 individual members of the AGCM simulations forced with the history of global observed SSTs. The data given by the blue curve are from 15 individual members of unforced coupled atmosphere–ocean model simulations. The observed trend value is indicated by the gray bar.

warming since 1950 is consistent with a GHG signal (e.g., Hurrell et al. 2004). As discussed in the introduction, this warming has also been implicated as a key source of the drying over the Sahel. Our experiments, using a fixed Indian Ocean positive SST anomaly (section 2c), however, do not support this latter hypothesis.

In the 40-member AGCM ensemble, rainfall increases across the central and eastern Sahel within 15°–20°N during JAS (Fig. 7, top panel). A dry signal does occur over the western Sahel, a subregion where Hastenrath and Wolter (1992) found empirical evidence for an Indian Ocean warming source of deficient rainy sea-

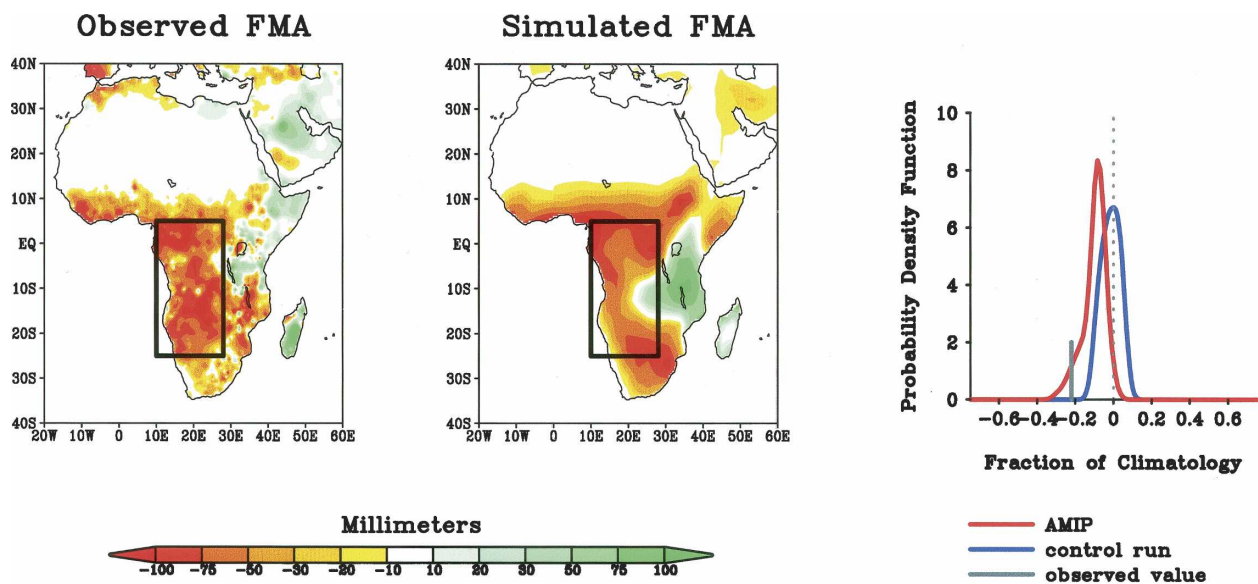


FIG. 6. Same as in Fig. 5, but for the FMA season. The PDFs are 50-yr rainfall trends averaged over the southern African region.

Indian Ocean Warming Effect

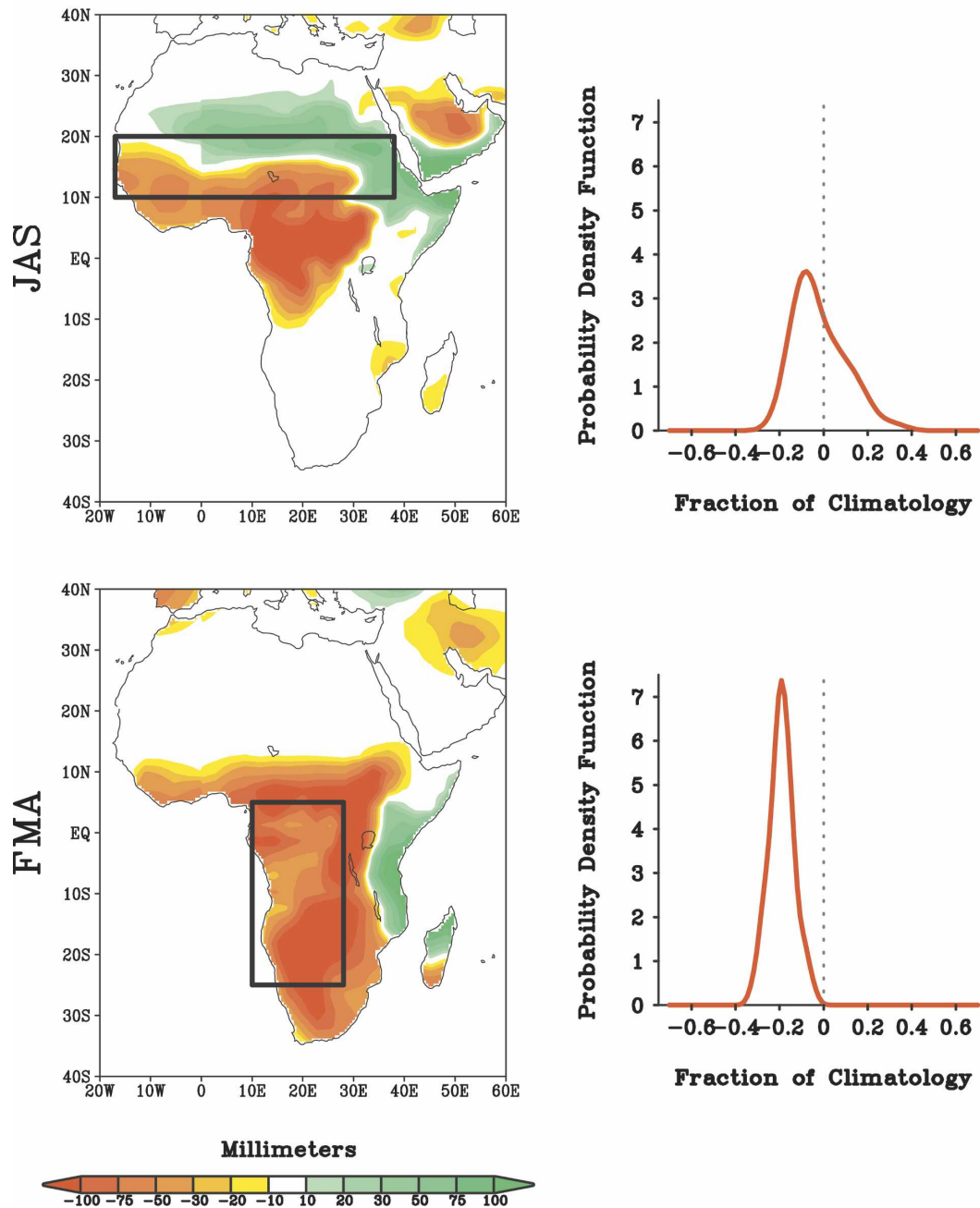


FIG. 7. Atmospheric GCM simulated African rainfall responses (mm) to a specified $+1^{\circ}\text{C}$ Indian Ocean sea surface warming during (top left) JAS and (bottom left) FMA. (right) Plots of the empirical PDFs of the seasonal rainfall response from the 40 individual members of the AGCM simulations.

sons, and where the experiments of Bader and Latif (2003) also suggested drying in response to Indian Ocean warming. The principal drying signal occurs in the more humid equatorial regions of central and western Africa, a response that appears consistent with an

anomalous Walker cell in which large-scale subsidence over equatorial Africa is linked to ascent and increased oceanic rainfall over the anomalously warm Indian Ocean (not shown).

The pattern correlations between the JAS rainfall

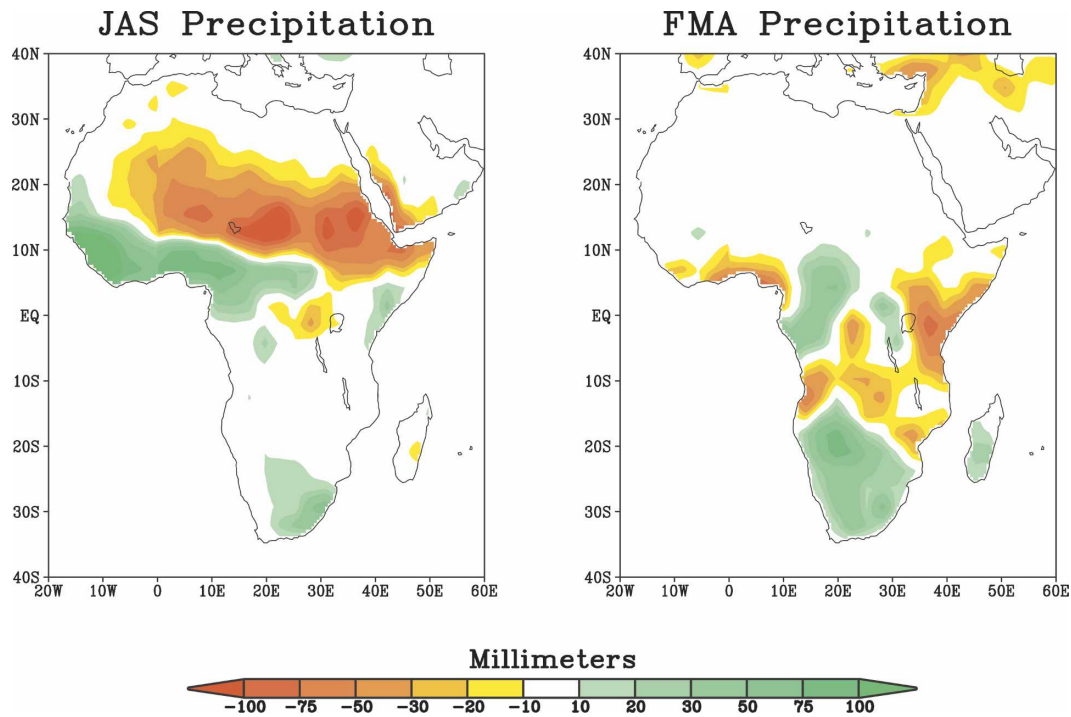


FIG. 8. The atmospheric GCM simulated 50-yr African rainfall trends for (left) JAS and (right) FMA. Rainfall is based on the monthly, gridded output of a 4-member ensemble average of a single atmospheric GCM that was forced by the time-varying, monthly observed SST variations over the Atlantic Ocean basin only. Plotted is the total seasonal rainfall change (mm) over the 50-yr period.

response to Indian Ocean warmth and the 1950–99 observed and AGCM rainfall trends are 0.1 and 0.0, respectively, for the map domain in Fig. 7. As further indication that Indian Ocean warmth is not a leading source for the Sahel drying occurring in our AGCM simulations forced by global SSTs, the PDF of the 40 individual JAS rainfall responses shows only a slight bias toward dryness (Fig. 7, top-right panel). This is in contrast to the PDF of Fig. 5 in which no single run under the influence of global SST forcing yielded a Sahel drying trend weaker than a -10% reduction of the climatological mean JAS value.

Indian Ocean warming does, however, induce widespread drying during austral summer over southern African (Fig. 7, bottom panel). The FMA response is strikingly similar to the 1950–99 FMA trend pattern itself (cf. Fig. 6). The spatial correlations of this response with the 1950–99 observed and AGCM rainfall trends are 0.5 and 0.6, respectively. Furthermore, virtually every member of the 40 simulations subjected to Indian Ocean warming yields below-normal southern African rainfall, analogous to the high reproducibility of 1950–99 drying trends in the AGCM runs that used global SST variations. We speculate that the mecha-

nism for this drying is a large-scale subsidence within a descending branch of an anomalous Walker circulation, whose ascending branch is located over the SH Indian Ocean where Hurrell et al. (2004) has shown both observational and modeling evidence for increased rainfall due to local SST warming.

These idealized Indian Ocean experiments reveal that, despite the tantalizing suggestion of a high Indian Ocean correlation with both southern and northern African drought (Figs. 1 and 4), only for the former region is a strong causal link verified. We find that the Sahel drying trend may have been more the consequence of fluctuations in Atlantic SSTs during the period. The 50-yr trend of JAS rainfall calculated from the four-member ensemble average of Atlantic-only SST simulations reveals widespread drying over most of the Sahel, juxtaposed with wet trends over the Guinea Coast (Fig. 8, left panel). This response captures several of the key features of the observed JAS rainfall trend (cf. Fig. 4), and is furthermore largely opposite to the JAS sensitivity to Indian Ocean warming. Note that no coherent trend in southern African rainfall occurs in response to the variations of the Atlantic SSTs (Fig. 8, right panel).

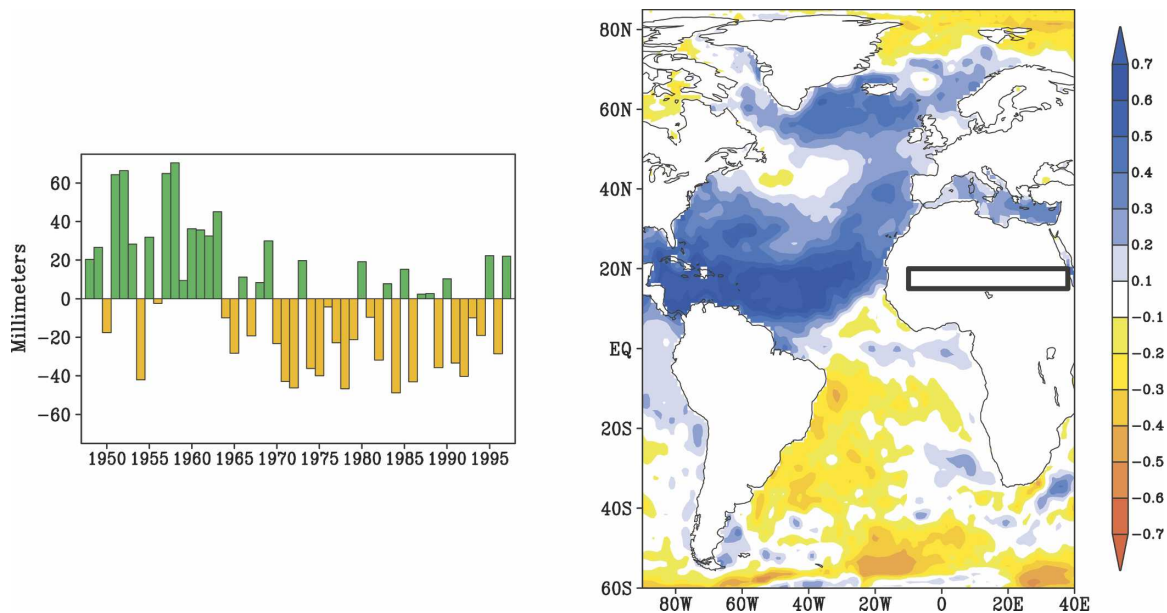


FIG. 9. The 50-yr seasonal time series of simulated rainfall departures (left) for JAS over northern Africa (right) from the Atlantic-only forced runs in Fig. 8. The spatial averaging region is indicated by the black box. The temporal correlation between the ensemble mean simulated rainfall time series and Atlantic basin SSTs for the JAS northern African rain season.

The time series of JAS rainfall in the Atlantic-only SST-forced simulations, sampling the zone within 15° – 20° N, 10° W– 38° E (Fig. 9, left panel), indicates two different rainfall regimes; one mostly wet before 1965 and the other mostly dry during the subsequent 30 yr. In this regard, the temporal history is reminiscent of observations for the Sahel region during 1950–99 (cf. Fig. 1). The linear correlation between this simulated time series and Atlantic basin SSTs (Fig. 9, right panel) reveals a characteristic structure that has been previously implicated as a source for Sahelian drought—the interhemispheric SST contrast in which the South Atlantic Ocean is warm relative to the North Atlantic (e.g., Folland et al. 1986; see also Ward 1998).

5. African monsoon rainfall response to GHG forcing

Our analysis of AGCM simulations reveals that a causal explanation for the observed 1950–99 African drying trends involves the role of oceans. The idealized SST-forced experiments identify two oceanic sources of importance, though an exhaustive analysis of all possible SST influences has not been performed. We have, for example, not addressed the role of variations in Pacific Ocean SSTs, such as those related to ENSO. On interannual time scales, ENSO is known to induce

an African rainfall response (e.g., Mason et al. 1999; Rowell 2001), and multidecadal variations in ENSO behavior could thus contribute to low-frequency changes in African rainfall.

Though largely attributable to oceanic forcing, the relative role of natural variability in the observed changes during 1950–99 could not be unequivocally determined from either the AGCM or coupled model experiments using fixed chemical constituents. We therefore examine suites of coupled models forced with estimates of changes in the atmosphere's chemical composition since 1950. We focus not only on the African rainfall response, but also on the SST response over the Indian and Atlantic Oceans, since both regions were demonstrated to be of particular importance for African drying during the latter half of the twentieth century.

a. Sahel rainfall

Shown in Fig. 10 (top panel) are the 1950–2049 GHG-forced JAS rainfall anomalies for the Sahel. The colored bars indicate the mean values of the 18 AR4 models, red crosses denote their median values, and the gray shading indicates the interquartile range. The time series is striking for two reasons. First, the GHG-forced signal over the Sahel is weak, especially during the twentieth century, although it is in qualitative agree-

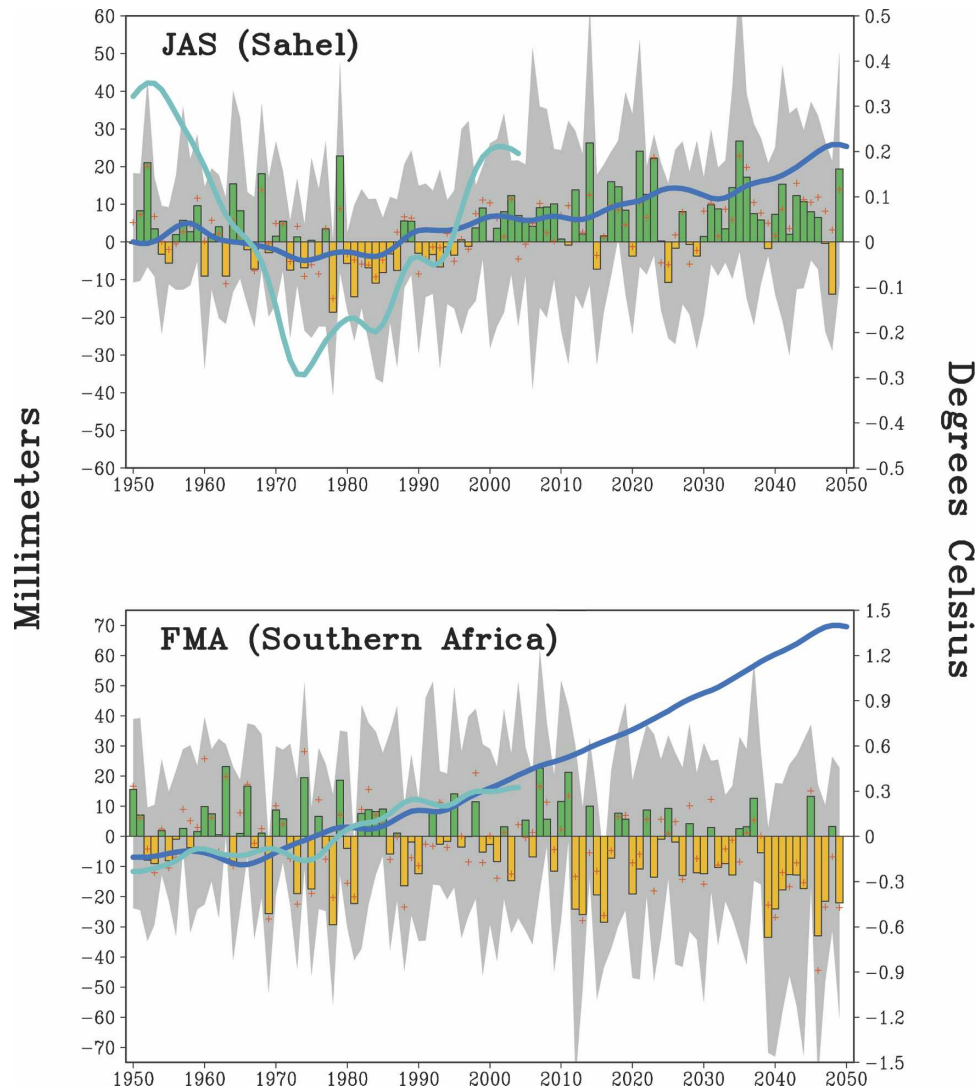


FIG. 10. GHG-forced simulated time series of (top) Sahel JAS and (bottom) southern African FMA seasonal rainfall departures for 1950–2049. Rainfall is based on the monthly, gridded output of the 18-model-averaged coupled atmosphere–ocean GCM runs collected from the IPCC/PCMDI AR4 database (see online at http://www-pcmdi.llnl.gov/ipcc/about_ipcc.php). Bars denote the average of the 18-model ensemble mean rainfall departures. Red crosses denote the median value of the 18-model ensembles. Gray shading signifies the interquartile range of the 18-model ensemble rainfall departures. Superimposed dark (light) blue curves are the projected (observed) SST time series of the (top) North Atlantic minus South Atlantic SST and (bottom) tropical Indian Ocean SST. The reference climatology is 1950–99.

ment with the observed decline (cf. Fig. 1). Second, there is a recovery in rainfall from a low point in the 1980s to values that consistently exceed the 1950–99 climatology after 2000.

To quantify the possible existence of an anthropogenic signal in the observed rainfall changes, we performed the following detection analysis (e.g., Barnett et al. 1999). The response pattern of the forced Sahel rain-

fall change is specified to be the 18-model average of the AR4 experiments. Denoting this as the “greenhouse fingerprint,” we project the observations upon this pattern over the Sahel domain. The projection coefficient is plotted on the abscissa of Fig. 11, while the amplitude of the GHG signal is plotted on the ordinate, expressed as the ratio of the area average simulated to observed rainfall trend. We repeat the analysis by pro-

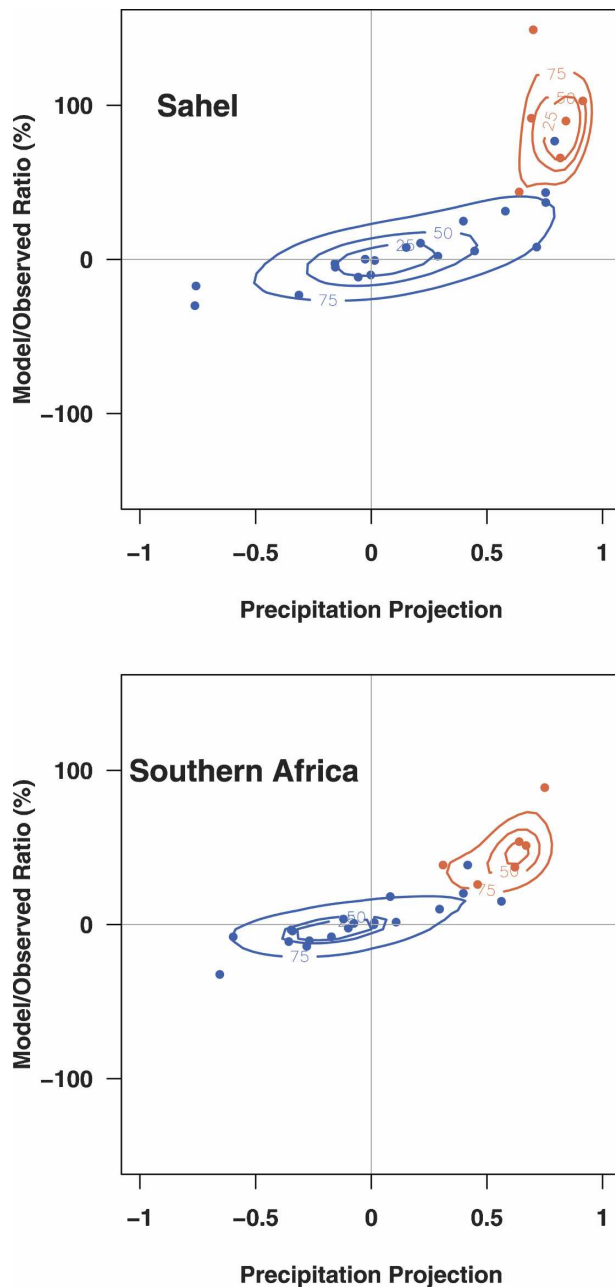


FIG. 11. Detection/attribution analysis for the observed 1950–99 50-yr rainfall trends over (top) the Sahel during JAS and (bottom) southern Africa during FMA. The greenhouse fingerprint and SST fingerprints are designated to be the pattern of rainfall trend in the 18-model average of the AR4, and the 5-model average of the Atmospheric Model Intercomparison Project (AMIP) experiments, respectively. Results based on designating each separate AR4 (AMIP) model as the greenhouse (SST) fingerprint are also shown. Blue (red) circles plot the two-dimensional coordinate of the projection of observed trends upon the greenhouse (SST) fingerprints (abscissa) together with their amplitude as a fraction of observed (ordinate), expressed in percent. Contours are of the probability densities,

projecting the observations upon each of the 18 AR4 model simulations separately in order to estimate signal uncertainty. The phase space probability densities of these results are contoured by the blue curves in Fig. 11.

The observed rainfall trend over the Sahel has virtually no projection upon the greenhouse fingerprint pattern of the 1950–99 change. Furthermore, this fingerprint pattern explains little of the observed amplitude change. Notable exceptions to the vast majority of individual points in this attribution space are those two which originate from very similarly configured Geophysical Fluid Dynamics Laboratory (GFDL) coupled models, whose GHG-forced signals project well onto the observed record (as further discussed below).

Also plotted in the attribution diagram are the probability densities that indicate the projection of the observed rainfall trend upon the “global SST fingerprint” derived from the five-AGCM-average simulated trends. Consistent with the PDF approach (section 3), these confirm the importance of the SST-forced signal, and further demonstrate the small uncertainty in signal detection as revealed by the agreement among the AGCMs. The minimal overlap between the two probability densities suggests that the observed global SSTs that drove Sahelian drying over the latter half of the twentieth century were not the consequence of GHG forcing.

The time-evolving GHG signal into the twenty-first century is one of increasing rainfall over the Sahel (Fig. 10). Although the spread of the rainfall changes is large, 14 of the 18 AR4 models simulate this increase. A similar result of northern African monsoon recovery was noted in the GHG experiments of Paeth and Hense (2004), and the AR4 results are furthermore in agreement with the GHG-forced simulations (involving 17 different models) performed as part of the IPCC Third Assessment Report (not shown). A few models, however, project a continuation of dry conditions over the Sahel into the future. Held et al. (2005) analyze the two (GFDL) models identified earlier (Fig. 11). It should be noted that despite being outliers among the 18 models, there is no a priori reason to discount the GFDL results. The fact that this particular model, forced with the observed GHG and aerosol changes during 1950–99 was able to reproduce the observed drying over the Sahel is intriguing, but further analysis of that model is beyond the scope of this paper.

While recognizing uncertainty in these projections there is a plausible *physical argument* for a wet Sahel rainfall signal because of GHG forcing. It is based on twentieth-century evidence that Sahel rainfall varies

interannually in tandem with the relative warmth of North Atlantic compared with South Atlantic SSTs (see the introduction). Our own attribution analysis for the twentieth century also found the low-frequency variations of Atlantic SSTs to be of primary importance. Superimposed on the rainfall in Fig. 10 is the time series of the GHG-forced signal in the interhemispheric SST contrast between the North and the South Atlantic (blue curve). The period of Sahel rainfall increase is synchronized with a progressive warming of the North Atlantic relative to the South Atlantic Ocean. This differential warming of the Atlantic is unanimous among the AR4 models, and we suspect it to be a leading factor in their collective wet response. The amplitude of this signal, derived from the average of all AR4 models, however, equates to an only +2% increase above the 1950–99 climatology by 2049. Such a 50-yr change signal could be readily masked by more intense unforced variations, whose one standard deviation is about 10% of climatology (see Fig. 5).

b. Southern African rainfall

The same detection analysis was also performed for southern Africa during the February–April season (Fig. 11, bottom panel). As for the Sahel, the observations exhibit no projection upon the GHG fingerprint pattern, nor does the fingerprint pattern explain the observed change in amplitude. The probability density function that contours the phase space of individual models is centered near the graph's origin, confirming the absence of a GHG-forced attributable cause.

The phase space of the GHG fingerprints is virtually independent of that associated with the global SST fingerprint. This would indicate that the observed SST forcing, which played a critical role in southern African drying, was itself not a consequence of GHG forcing. Yet, such an interpretation contradicts our finding (section 4) that the observed Indian Ocean warming was the immediate cause for the drying simulated in the AGCMs, and that such warming was directly attributable to twentieth-century GHG changes (Hurrell et al. 2004; also see below). It is possible that other GHG-forced changes in SSTs outside of the Indian Ocean region differ from the observed changes, and that these act to mask the Indian Ocean drying effect during 1950–99. It is also possible that mean biases in the SST climatologies of the AR4 models alter their sensitivity to Indian Ocean warming compared with “perfect ocean” AGCM simulations. Both of these possibilities are the focus of additional ongoing research.

During the twenty-first century, southern Africa falls

within the epicenter of a GHG-forced dry signal. As shown in the appendix (Fig. A3), this drying is most prominent over a region south of 10°S during the FMA season, whereas a wet signal occurs to the north, and also over eastern Africa. This pattern of change is reminiscent of the observed twentieth-century trend during austral summer, though the drying is more regionally confined to southern Africa. It furthermore resembles the pattern of change simulated as the atmospheric response to specified isolated Indian Ocean warmth (cf. Fig. 7).

The 1950–2049 GHG-forced rainfall time series computed over a smaller domain of southern Africa (15°–30°S, 15°–35°E) displays the increased frequency and severity of dry rainfall seasons during the twenty-first century (Fig. 10, bottom panel). Though there is considerable spread among the 18 models, the majority project a decline in rainfall. The ensemble average yields a –5% decline during 2000–49, which is nearly equal to the estimated one standardized departure of unforced 50-yr rainfall variations (see Fig. 6).

The superposed curve in Fig. 10 shows the ensemble averaged Indian Ocean SST response to GHG forcing, and it reveals a linear warming, emerging after 1970. Given our earlier evidence for a causal link between Indian Ocean warming and drought over southern Africa during 1950–99, the projected twenty-first-century drying there may be a consequence of the expected further Indian Ocean warming. As mentioned earlier, it is perplexing that the ensemble average of AR4 simulations does not yield a southern African drying trend during 1950–99, given the fact that the amplitude and timing of observed twentieth-century Indian Ocean warming is well simulated. Thus, additional diagnostics are required to confirm that the projected twenty-first-century Indian Ocean warming is the immediate physical cause for the projected drying over southern Africa.

6. Outstanding questions

Among the requests for climate information by decision makers is an explanation of the current climate system. Not a description alone—though accurate accounting of past and current climate states is important—but an essential causal understanding. In this study we have sought the causes for sustained late-twentieth-century African drought. Best known of these is the drying of the Sahel in the decades after 1970, but also of great consequence has been southern African drying occurring simultaneously. The scientific challenges are well articulated by the pressing questions

of regional decision makers. Are such droughts the rare events expected from and embodied within the natural swings of climate? Are the factors responsible for their occurrence expected to occur more frequently in the future? The discussion below is therefore framed within specific questions on the African drying trends during 1950–99.

a. Is there an attributable cause for the post-1950 African drying trends?

Our diagnosis of atmospheric models revealed that the 1950–99 African drying trends were directly attributable to fluctuations in the observed global SST field. A trajectory toward drying during this half-century was wholly determined by SST influences in so far as virtually every simulation, derived from 80 experiments spanning five different AGCMs, produced a drying trend. As one test of the robustness of that attribution owing to signal uncertainty, the trend of each separate AGCM ensemble was computed, and the reproducibility of high pattern correlations between the observed trend and modeled trends was found for each.

Regarding the question of which SSTs were most consequential to African drying, our diagnosis indicated that the relative cooling of the tropical North Atlantic compared with the tropical South Atlantic over the last half of the twentieth century was the key driver of drought over the Sahel. The models examined failed to support the hypothesis of a causal link between Indian Ocean warming and the widespread Sahelian drought as proposed in Giannini et al. (2003) and Bader and Latif (2003). The relevance of Indian Ocean warmth for Sahel rainfall remains an open question, however. The sensitivity of the two AGCMs examined herein differs from that of two different AGCMs used in Bader and Latif (2003) and Lu and Delworth (2005). As further discussed below, understanding if and how Indian Ocean warming affects the Sahel may be key toward advancing confidence in projections of twenty-first-century rainfall changes over the region.

On the other hand, Indian Ocean warmth exerts a strong drying effect over southern Africa during austral summer. This latter drying signal can be understood as resulting from a large-scale subsidence that is coupled to a convectively driven ascent over the anomalously warm Indian Ocean. Confidence in this conclusion is high owing to the remarkable correspondence between the southern African rainfall response to idealized Indian Ocean warmth and to the observed global SST variations, and also by our ability to reproduce those sensitivities in additional experiments employing different AGCMs (not shown).

b. What role did GHG forcing play in the 1950–99 African drying trends?

We took two approaches to determine the role of forcings external to the naturally occurring fluctuations of the coupled ocean–atmosphere system. First, we inquired whether the observed changes could have occurred because of natural variability. African rainfall trends of 50-yr duration simulated in unforced coupled models were examined. Though these models failed to produce any statistical occurrences of monsoon drying of the strength observed, we believe this is because of their deficiencies rather than a true indication for a restricted range in naturally occurring African rainfall fluctuations. Direct estimation of the natural variability is not possible from the brief instrumental record, though it is noteworthy that the recent African dryings appear to be neither unusual nor extreme from a paleoclimate perspective of natural variability (Verschuren et al. 2000; deMenocal 2004). Therein, the “total” variability includes, beyond the factors implicit in the aforementioned modern-era coupled simulations, possible changes in external forcings involving solar output and orbital parameters.

Second, we examined the simulated 1950–99 rainfall trends occurring in the AR4 models. We conducted a detection analysis in which the GHG fingerprint was chosen to be the 18-model ensemble response to observed GHG changes during 1950–99. We then quantified the anthropogenic component of observed African rainfall changes by projecting the observations upon this fingerprint. There was no projection of the observed 1950–99 rainfall trend over southern Africa onto the GHG-forced trend. Over the Sahel, a small positive projection of the spatial pattern of the observed trend onto the GHG signal of the 18-model average was found, but this was a result of the sensitivity of only two models. For both regions, the observed trend amplitude exceeded that of the GHG signal by an order of magnitude. We therefore concluded that GHG forcing played little or no role in the 1950–99 observed African drying trends.

c. Is African rainfall sensitive to GHG forcing?

Our analysis of the 1950–2049 AR4 simulated African rainfall time series highlighted two coherent, though opposite signed, GHG-induced signals emergent during the twenty-first century. One was a wet trend over the Sahel, with virtually every year after 2000 yielding a positive rainfall departure, and 14 of 18 AR4 models projecting such a trend. This twenty-first-century wet signal occurs in lockstep with projected

increasing warmth of North Atlantic relative to South Atlantic SSTs. We propose that the physical cause of this GHG-forced Sahelian wet signal is analogous to that contributing to the observed dry trend during 1950–99, namely, the region’s sensitivity to the meridional gradient of Atlantic basin SSTs. An important unresolved issue concerns the impact of Indian Ocean warming in particular, and a more general global sea surface warming as a whole as discussed in Held et al. (2005). It is plausible that the few, outlier AR4 models that predict further Sahelian drying during the twenty-first century are among the most sensitive to Indian Ocean warming, with a resulting dry signal dominating the wet influence of the change in meridional SST gradients across the Atlantic basin.

A second coherent-projected GHG-forced signal was a drying trend over southern Africa, with almost all years after 2000 yielding a negative rainfall departure compared with the 1950–99 reference climatology. This projected drying occurs in tandem with projected Indian Ocean warming. Our interpretation was that the latter oceanic change, which is unanimous across all AR4 models, is a contributing factor for this GHG-forced drying signal, as supported by our finding of a similar regionally focused drying occurring in atmospheric models subjected to isolated Indian Ocean warmth.

7. Concluding remarks

Our understanding of the broad sweep of climate model experiments studied herein is that the late-twentieth-century drying trend over the Sahel was likely due to natural causes and has not been a harbinger for human-induced climate change of oceanic origins. Furthermore, whereas the GHG-forced trend signal of 2000–49 Sahel rainfall is wet, its small amplitude suggests that natural variability will continue to be the primary driver of that region’s low-frequency rainfall variations during the next century. The southern African drying during 1950–99 was also likely a result of natural variability, although the ensemble of AR4 projections indicate this region to be at risk for increased drought during the twenty-first century. We find that an accelerated drying through the mid-twenty-first century occurs not only in the February–April season, but virtually throughout the entire seasonal cycle over southern Africa, with the GHG-signal amplitude of 50-yr change nearly equal to our estimated standard deviation of naturally occurring 50-yr trends.

While recognizing the uncertainty in the AR4 African rainfall projections for the twenty-first century,

they have some support from a physical understanding of that region’s sensitivity to oceanic influences that led to twentieth-century drought. A projected northern Africa wet GHG signal is consistent with a projected warming of North Atlantic SSTs relative to the South Atlantic. A southern African dry signal is consistent with an expected ongoing warming trend of the Indian Ocean. These interpretations need to be weighed against other important open questions of relevance to African rainfall sensitivity that have not been considered in this paper. In particular, our analysis has not given a comprehensive assessment of all oceanic influences, nor of other boundary influences including land surface and soil moisture changes. Nor has our study addressed the direct effects of aerosols on African climate. It should also be noted that effects on African rainfall could occur through dynamical or thermodynamical influences that do not involve ocean changes, and these may in fact mask or enhance oceanic influences.

Nonetheless, the simple framework of the sensitivity to two particular oceanic regions, building upon a rich history of prior research on African rainfall variability, has clarified the different effects of each ocean on northern and southern Africa since 1950. It emphasizes that future trajectories of these oceans may be important in defining regional rainfall change over Africa. One question, raised by the results of this study, is whether a so-called “maximum likelihood” state of African monsoon rainfall can be determined that is based on knowledge of the most probable mean change in SSTs. It is expected that further diagnosis of physical processes underlying the teleconnective response of African climate to SST forcing will be a key toward advanced understanding and improving predictions.

Acknowledgments. We thank the anonymous reviewers for their helpful comments on an earlier draft of this paper. We are grateful for the model data provided by P. Pegion, S. Schubert, M. Suarez, and C. Cassou. We also acknowledge the assistance of G. Bates and T. Xu. Support for this work was provided by the CLIVAR Program of the NOAA/Office of Global Programs.

APPENDIX

Seasonal Cycle of African Rainfall Trends

Shown are the complete seasonal cycles of African rainfall trends observed for 1950–99 (Fig. A1), simulated as a response to the known global SST and sea ice variations for 1950–99 (Fig. A2), and projected as a response to GHG forcing for 2000–49 (Fig. A3).

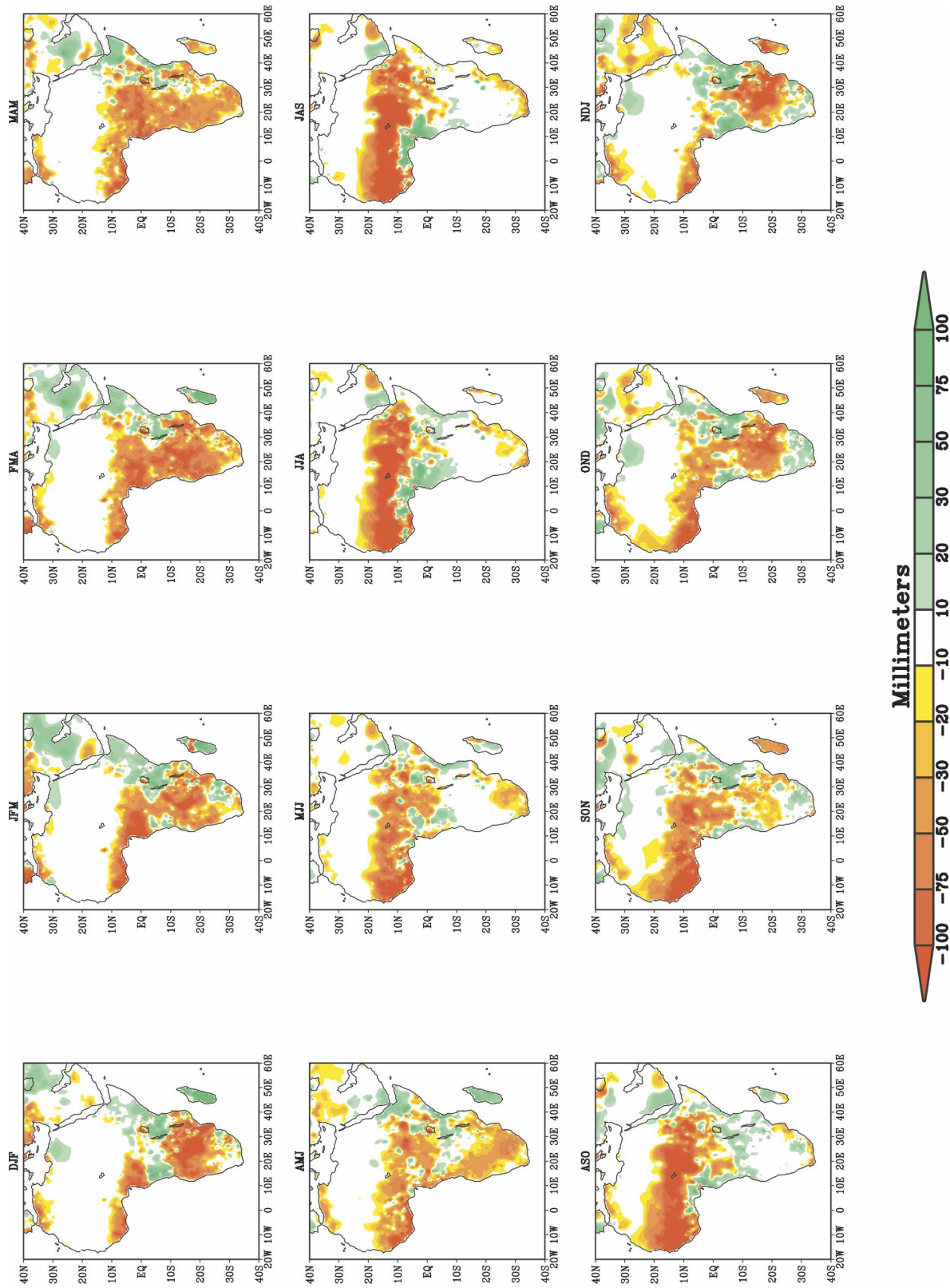


FIG. A1. The seasonal cycle of the observed 50-yr rainfall trends for 1950-99. Plotted is the total seasonal rainfall change (mm) over the 50-yr period for each of the 12 overlapping seasons. Rainfall is based on the monthly, 0.5° gridded analyses from the University of Delaware.

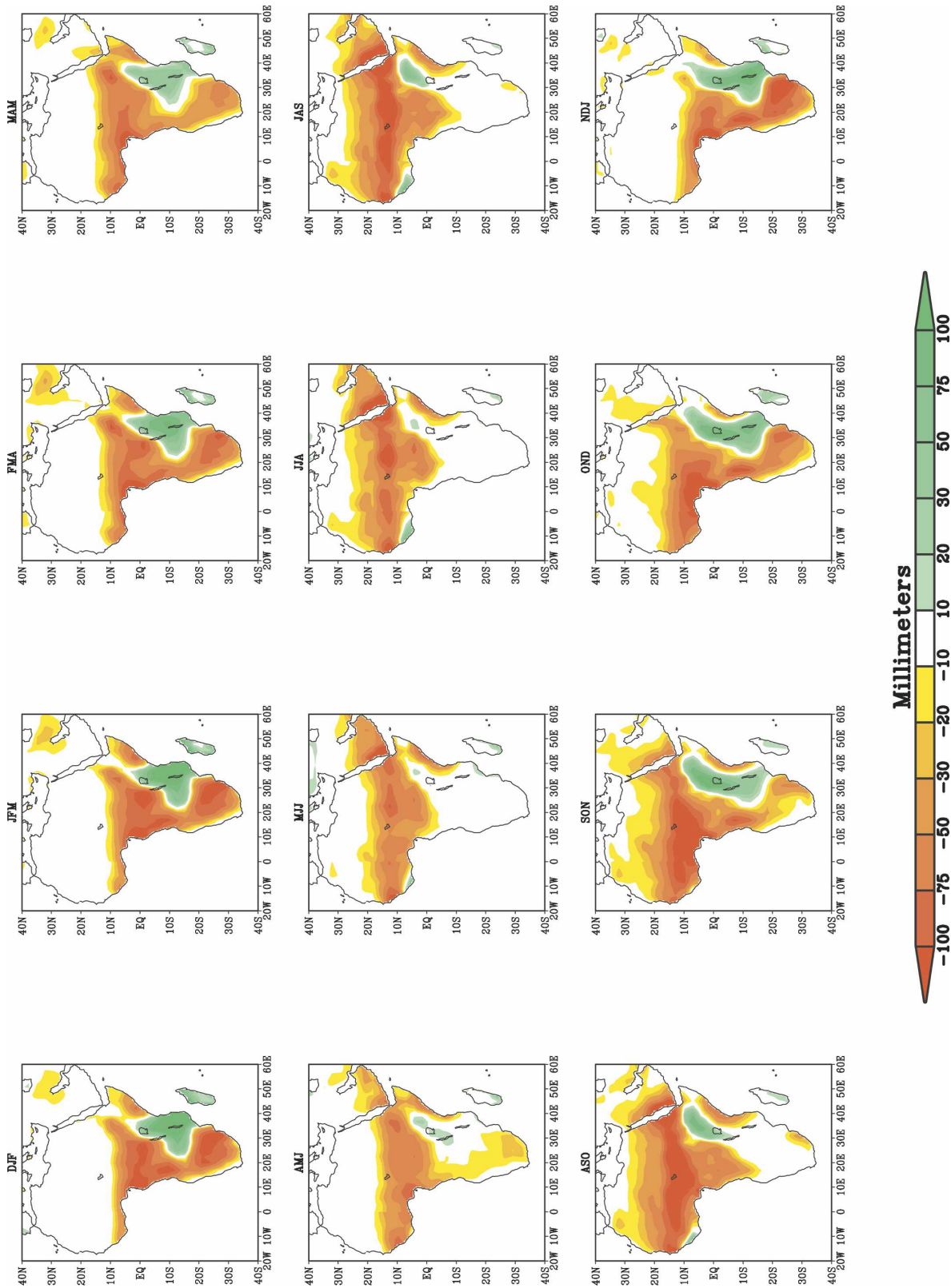


FIG. A2. The seasonal cycle of the AGCM simulated 50-yr rainfall trends for 1950–99. Plotted is the total seasonal rainfall change (mm) over the 50-yr period for each of the 12 overlapping seasons. Rainfall is based on the monthly, gridded output of the five-model, 80-member ensemble average of AGCM runs forced with observed monthly varying global SST and sea ice variations.

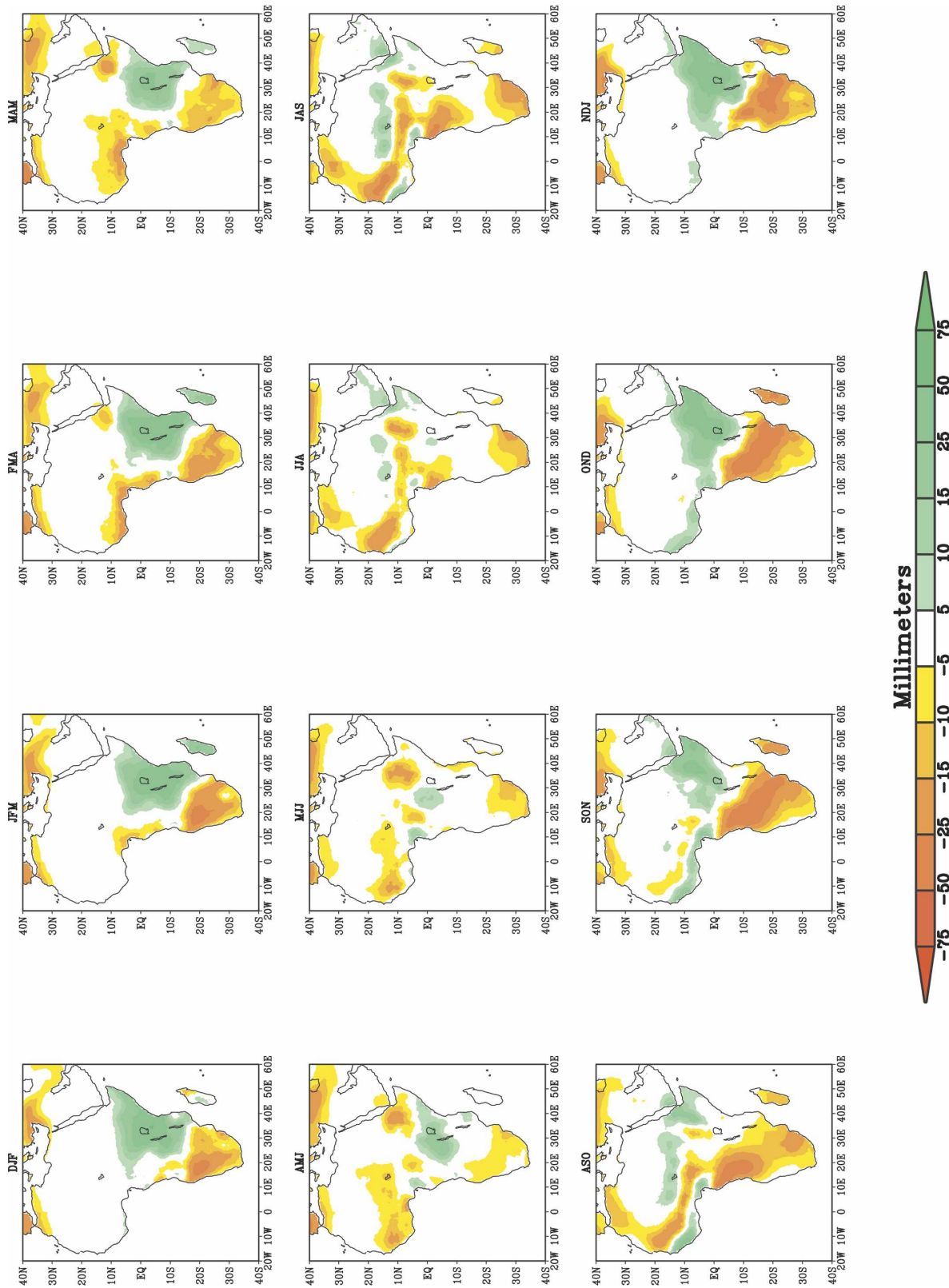


FIG. A3. The seasonal cycle of GHG-forced simulated 50-yr rainfall trends for 2000–49. Plotted is the total seasonal rainfall change (mm) over the 50-yr period for each of the 12 overlapping seasons. Rainfall is based on the monthly, gridded output of the 18-model, 42-member ensemble average of coupled atmosphere–ocean GCM runs collected from the IPCC/PCMDI AR4 database (see online at http://www.pcmdi.llnl.gov/ipcc/about_ipcc.php).

REFERENCES

- Achutarao, K., and K. Sperber, 2002: Simulation of El Niño/Southern Oscillation: Results from the coupled model inter-comparison project. *Climate Dyn.*, **19**, 191–209.
- Bader, J., and M. Latif, 2003: The impact of decadal-scale Indian Ocean sea surface temperature anomalies on Sahelian rainfall and the North Atlantic Oscillation. *Geophys. Res. Lett.*, **30**, 2169, doi:10.1029/2003GL018426.
- Barnett, T. P., 1999: Comparison of near-surface air temperature variability in 11 coupled global climate models. *J. Climate*, **12**, 511–518.
- , and Coauthors, 1999: Detection and attribution of recent climate change: A status report. *Bull. Amer. Meteor. Soc.*, **80**, 2631–2659.
- , D. Pierce, K. Achutarao, P. Gleckler, B. Santer, J. Gregory, and W. Washington, 2005: Penetration of human-induced warming into the world's oceans. *Science*, **309**, 284–287.
- Cassou, C., and L. Terray, 2001: Dual influence of Atlantic and Pacific SST anomalies on the North Atlantic/Europe winter climate. *Geophys. Res. Lett.*, **28**, 3195–3198.
- deMenocal, P. B., 2004: African climate change and faunal evolution during the Pliocene-Pleistocene. *Earth Planet. Sci. Lett.*, **220**, 3–24.
- Folland, C. K., T. N. Palmer, and D. E. Parker, 1986: Sahelian rainfall and worldwide sea temperatures 1901–1985. *Nature*, **320**, 602–607.
- Giannini, A., R. Saravanan, and P. Chang, 2003: Oceanic forcing of Sahel rainfall on interannual to interdecadal time scales. *Science*, **302**, 1027–1030.
- Goddard, L., and N. E. Graham, 1999: The importance of the Indian Ocean for simulating rainfall anomalies over eastern and southern Africa. *J. Geophys. Res.*, **104**, 19 099–19 116.
- Gregory, J. M., and J. A. Lowe, 2000: Predictions of global and regional sea level rise using AOGCMs with and without flux adjustment. *Geophys. Res. Lett.*, **27**, 3069–3072.
- Hastenrath, S., 1984: Interannual variability and annual cycle: Mechanisms of circulation and climate in the tropical Atlantic sector. *Mon. Wea. Rev.*, **112**, 1097–1107.
- , and K. Wolter, 1992: Large-scale patterns and long term trends of circulation variability associated with Sahel rainfall anomalies. *J. Meteor. Soc. Japan*, **70**, 1045–1055.
- Held, I. M., T. L. Delworth, J. Lu, K. L. Findell, and T. R. Knutson, 2005: Simulation of Sahel drought in the 20th and 21st centuries. *Proc. Natl. Acad. Sci.*, **102**, 17 891–17 896.
- Hirst, A. C., and S. Hastenrath, 1983: Atmosphere–ocean mechanisms of climate anomalies in the Angola–tropical sector. *J. Phys. Oceanogr.*, **13**, 1146–1157.
- Houghton, J. T., Y. Ding, D. J. Griggs, M. Noguer, P. J. van der Linden, and D. Xiaosu, Eds., 2001: *Climate Change 2001: The Scientific Basis*. Cambridge University Press, 944 pp.
- Hulme, M., 1996: Recent climatic change in the world's drylands. *Geophys. Res. Lett.*, **23**, 61–64.
- Hurrell, J. W., M. P. Hoerling, A. Phillips, and T. Xu, 2004: Twentieth century North Atlantic climate change. Part I: Assessing determinism. *Climate Dyn.*, **23**, 375–390.
- Kiehl, J. T., and P. J. Gent, 2004: The Community Climate System Model, version 2. *J. Climate*, **17**, 3666–3682.
- Knutson, T. R., T. L. Delworth, K. W. Dixon, and R. J. Stouffer, 1999: Model assessment of regional surface temperature trends (1949–1997). *J. Geophys. Res.*, **104**, 30 981–30 996.
- Lamb, P. J., 1978a: Case studies of tropical Atlantic surface circulation patterns during recent Subsaharan weather anomalies: 1967 and 1968. *Mon. Wea. Rev.*, **106**, 482–491.
- , 1978b: Large-scale tropical Atlantic surface circulation patterns associated with Subsaharan weather anomalies. *Tellus*, **30A**, 240–251.
- Landman, W. A., and L. Goddard, 2002: Statistical recalibration of GCM forecasts over southern Africa using model output statistics. *J. Climate*, **15**, 2038–2055.
- Legates, D. R., and C. J. Willmott, 1990: Mean seasonal and spatial variability in gauge-corrected, global precipitation. *Int. J. Climatol.*, **10**, 111–127.
- Lu, J., and T. Delworth, 2005: Oceanic forcing of the late 20th century Sahel drought. *Geophys. Res. Lett.*, **32**, L22706, doi:10.1029/2005GL023316.
- Mason, S. J., L. Goddard, N. E. Graham, E. Yelaeva, L. Sun, and P. A. Arkin, 1999: The IRI seasonal climate prediction system and the 1997/98 El Niño event. *Bull. Amer. Meteor. Soc.*, **80**, 1853–1873.
- Paeth, H., and A. Hense, 2004: SST versus climate change signals in west African rainfall: 20th Century variations and future projections. *Climate Change*, **65**, 179–208.
- Palmer, T. N., 1986: The influence of Atlantic, Pacific, and Indian Oceans on Sahel rainfall. *Nature*, **322**, 251–253.
- Rayner, N. A., D. E. Parker, E. B. Horton, C. K. Folland, L. V. Alexander, D. P. Rowell, E. C. Kent, and A. Kaplan, 2003: Global analyses of sea surface temperature, sea ice, and night marine air temperature since the late nineteenth century. *J. Geophys. Res.*, **108**, 4407, doi:10.1029/2002JD002670.
- Roeckner, E., and Coauthors, 1992: Simulation of the present-day climate with the ECHAM model: Impact of model physics and resolution. Max Planck Institute für Meteorologie Rep. 93, Hamburg, Germany, 171 pp.
- , and Coauthors, 1996: The atmospheric general circulation model ECHAM4: Model description and simulation of present-day climate. Max Planck Institute für Meteorologie Rep. 218, Hamburg, Germany, 90 pp.
- , L. Bengtsson, J. Feichter, L. Lelieveld, and H. Rodhe, 1999: Transient climate change simulations with a coupled atmosphere–ocean GCM including the tropospheric sulfur cycle. *J. Climate*, **12**, 3004–3032.
- Rouault, S. A., C. J. White, C. Reason, J. Lutjeharms, and I. Jobard, 2002: Ocean–atmosphere interaction and a South African extreme weather event. *Wea. Forecasting*, **17**, 655–669.
- Rowell, D. P., 2001: Teleconnections between the tropical Pacific and the Sahel. *Quart. J. Roy. Meteor. Soc.*, **127**, 1683–1706.
- , C. Folland, K. Makell, and N. Ward, 1995: Variability of summer rainfall over tropical North Africa (1906–92): Observations and modelling. *Quart. J. Roy. Meteor. Soc.*, **121**, 669–704.
- Schubert, S. D., M. J. Suarez, P. J. Pegion, R. D. Koster, and J. T. Bacmeister, 2004: Causes of long-term drought in the U.S. Great Plains. *J. Climate*, **17**, 485–503.
- Stott, P. A., S. F. B. Tett, G. S. Jones, M. R. Allen, J. B. Mithell, and G. J. Jenkins, 2000: External control of 20th Century temperature by natural and anthropogenic forcings. *Nature*, **290**, 2133–2137.
- Verschuren, D., K. R. Laird, and B. F. Cumming, 2000: Rainfall and drought in equatorial east Africa during the past 1100 years. *Nature*, **403**, 410–414.
- Ward, N. W., 1998: Diagnosis and short-lead prediction of summer rainfall in tropical North Africa at interannual and multi-decadal timescales. *J. Climate*, **11**, 3167–3191.
- Willmott, C. J., and S. M. Robeson, 1995: Climatologically aided interpolation (CAI) of terrestrial air temperature. *Int. J. Climatol.*, **15** (2), 221–229.